GLIA WILEY

Axoglial synapses are formed onto pioneer oligodendrocyte precursor cells at the onset of spinal cord gliogenesis

Guillaume Osterstock[1] | Barbara Le Bras[1] | Kalaimakan Hervé Arulkandarajah[1] | Hervé Le Corronc[1,2] | Antonny Czarnecki[1] | Christine Mouffle[1] | Erika Bullier[1] | Pascal Legendre[1] | Jean-Marie Mangin[1]

[1]Sorbonne Université, UM119, Neuroscience Paris Seine, Paris F-75005, France Centre National de la Recherche Scientifique (CNRS), UMR 8246, Paris F-75005, France Institut National de la Santé et de la Recherche Médicale (INSERM), U1130, Paris, F-75005, France

[2]Université d'Angers, Angers, 49000, France

Correspondence
Jean-Marie Mangin, Laboratoire Neuroscience Paris Seine, 7-9 Quai Saint Bernard, 75005 Paris, France.
Email: jean-marie.mangin@inserm.fr

Funding information
Agence Nationale de la Recherche, Grant/Award Number: ANR-11-JSV4-002-01; Institut de Recherche sur la Moelle et l'encéphale; AFM-Telethon; Fondation pour la Recherche Médicale

Abstract

Virtually all oligodendrocyte precursors cells (OPCs) receive glutamatergic and/or GABAergic synapses that are lost upon their differentiation into oligodendrocytes in the postnatal and adult brain. Although OPCs are generated at mid-embryonic stages, several weeks before the onset of myelination, it remains unknown when and where OPCs receive their first synapses and become susceptible to the influence of neuronal activity. In the embryonic spinal cord, neuro-epithelial precursors in the pMN domain cease generating cholinergic motor neurons (MNs) to produce OPCs when the first synapses are formed in the ventral-lateral marginal zone. We discovered that when the first synapses form onto MNs, axoglial synapses also form onto the processes of neuro-epithelial precursors located in the marginal zone as they differentiate into OPCs. After leaving the neuro-epithelium, these pioneer OPCs preferentially accumulate in the marginal zone where they are contacted by functional glutamatergic and GABAergic synapses. Spontaneous activity of these axoglial synapses was significantly potentiated by cholinergic signaling acting through presynaptic nicotinic acetylcholine receptors. Moreover, we discovered that chronic nicotine treatment significantly increases early OPC proliferation and density in the marginal zone. Our results demonstrate that OPCs are contacted by functional synapses as soon as they emerge from their precursor domain and that embryonic spinal cord colonization by OPCs can be regulated by cholinergic signaling acting onto these axoglial synapses.

KEYWORDS
development, electrophysiology, neural precursor, oligodendrocyte

1 | INTRODUCTION

Oligodendrocyte progenitor cells (OPCs) are a subpopulation of glial cells known to give rise to most if not all myelinating oligodendrocytes, both during development and after a demyelinating injury in the postnatal and adult brain (Bergles & Richardson, 2016). One of the most intriguing property of brain OPCs is their ability to receive glutamatergic and GABAergic synapses from neurons, both in the grey (Bergles, Roberts, Somogyi, & Jahr, 2000; Lin & Bergles, 2004; Mangin, Kunze, Chittajallu, & Gallo, 2008) and white matter areas (Etxeberria, Mangin, Aguirre, & Gallo, 2010; Kukley, Capetillo-Zarate, & Dietrich, 2007; Sahel et al., 2015; Ziskin, Nishiyama, Rubio, Fukaya, & Bergles, 2007). Axoglial synapses appear to be a universal feature of OPCs in

the mammalian postnatal and adult brain and they have been reported in all brain areas investigated so far - hippocampus, cortex, cerebellum, brainstem, corpus callosum and optic nerve (Gallo, Mangin, Kukley, & Dietrich, 2008; Hill & Nishiyama, 2014; Lin & Bergles, 2004). Because axoglial synapses are formed *de novo* during remyelination (Etxeberria et al., 2010; Sahel et al., 2015) and are lost upon differentiation into oligodendrocytes (De Biase, Nishiyama, & Bergles, 2010; Kukley, Nishiyama, & Dietrich, 2010), it has been suggested that they play a specific role during the early steps of the myelination/remyelination process at postnatal and adult stages (Etxeberria et al., 2010; Gallo et al., 2008; Paukert & Bergles, 2006; Sahel et al., 2015). However, OPCs are generated from their precursor domains at mid-embryonic stages, several weeks before the onset of myelination (Rowitch, 2004)

and it still remains unknown whether these pioneer OPCs could already be under the influence of axoglial transmission at such early stages, when they start colonizing the central nervous system.

The two earliest markers of OPCs are the chondroitin sulfate proteoglycan NG2 and the platelet-derived growth factor receptor A (PDGFRα; Nishiyama, Lin, Giese, Heldin, & Stallcup, 1996; Pringle & Richardson, 1993). In the mouse spinal cord, these two markers first appear around the 12th embryonic day of development (E12) in a restricted domain of the ventricular zone (VZ) lining the central canal known as the pMN domain (for precursor of Motor Neurons). The pMN domain, characterized by the expression of the olig2 transcription factor, contains neuro-epithelial precursors which switch from motor neuron (MN) genesis to OPC production around E12. However, the molecular and cellular mechanism(s) triggering and regulating this event are still not fully understood. In the embryonic spinal cord, synaptogenesis also starts around E12 when longitudinal axons from GABAergic and glutamatergic spinal interneurons (INs) form their first synapses onto MN dendrites located in the marginal zone (MZ; Czarnecki et al., 2014; Scain et al., 2010; Vaughn, Henrikson, & Grieshaber, 1974).

In the present study, we found that, at E12, the first OPCs expressing NG2 in the pMN domain exhibit radial processes that cross the ventral parenchyma to reach the MZ near the motor exit point (MEP), where MN axons exit the spinal cord. During the next two days, as they leave the neuro-epithelium to colonize the ventral spinal cord, the cell bodies of these pioneer OPCs were found to preferentially accumulate around the MEP. By performing patch-clamp recordings in whole embryonic spinal cord preparation, we found that these pioneer OPCs formed functional synapses with glutamatergic and GABAergic axons as soon as their soma invaded the marginal zone. In addition, electron microscopy showed that synaptic-like axoglial contacts are already forming onto neuro-epithelial precursor endfeet located around the MEP at E12. Although OPCs did not express any functional nicotinic acetylcholine receptor (nAChR), both glutamatergic and GABAergic synaptic inputs were significantly potentiated by exogenous acetylcholine acting through presynaptic nAChRs. The application of nAChR antagonist was found to significantly depress only GABAergic evoked currents and spontaneous GABAergic synaptic activity, showing that endogenous cholinergic signaling preferentially potentiate early GABAergic axoglial inputs onto OPCs. Finally, we found that chronic administration of nicotine during the onset of gliogenesis significantly increased OPC density and proliferation in the ventral spinal cord.

2 | MATERIALS AND METHODS

2.1 | Isolated embryonic spinal cord preparation

All experiments were performed in accordance with European Community guiding principles on the care and use of animals (86/609/CEE, CE Off J L358, December 18, 1986), the French decree 97/748 of October 19, 1987 (J Off République Française, October 20, 1987, pp. 12245–12248), and the recommendations from the Centre National de la Recherche Scientifique. C57BL/6 mice expressing an enhanced green fluorescence protein (EGFP) driven by cyclic nucleotide 3- phosphodiesterase promoters (CNP-EGFP) in oligodendroglial cells (Yuan et al., 2002) were crossed with 8–12-week-old Swiss mice (Janvier labs, Le Genest-Saint-Isle, France). Embryonic mouse spinal cords were dissected as previously described (Czarnecki et al., 2014). Briefly, pregnant mice were killed using a lethal dose of CO_2 followed by cervical dislocation. Mice embryos of both sexes were removed and quickly observed under a 470–515 nm excitation light using a fluorescence stereo-microscope (Leica MZ FLIII, Wetzlar, Germany) to identify EGFP-expressing embryos. The SC was isolated from EGFP positive embryos. Whole SCs were then incubated for 1 hr at 37°C in ACSF containing 126 mM NaCl, 25 mM NaHCO3, 10 mM glucose, 4.5 mM KCl, 2 mM CaCl2, 1.2 mM NaH2PO4, and 1 mM MgCl2 (325 mosmol/ kg H2O), continuously bubbled with a 95% O_2–5% CO_2 gas mixture.

2.2 | Patch-clamp recordings

The isolated spinal cord was placed in a recording chamber and continuously perfused (2 ml/min) at room temperature (20°C–24°C) with the oxygenated ACSF described above. Whole-cell voltage-clamp recordings of CNP-EGFP cells were performed under direct visualization using an infrared-sensitive CCD video camera. In addition to their GFP fluorescence, OPCs were distinguished based on their location inside the marginal zone, their elongated morphology and the presence of I_A and I_{KDR} voltage-dependent currents. To confirm their OPC identity, some recorded cells were filled with neurobiotin (1 mg/ml) and revealed in combination with NG2 immunostaining ($N = 6/6$). Whole-cell patch-clamp electrodes were pulled from thick-wall borosilicate glass using a Brown-Flaming puller (Sutter Instrument, Novato, CA, USA). Patch-clamp electrodes had resistances of 5–7 MΩ. For voltage-clamp experiments, the electrode was filled with a solution containing the following: 130 mM K-gluconate, 4 mM NaCl, 10 mM EGTA, 10 mM HEPES, 4 mM $MgCl_2$, 4 mM Na_2 ATP, 0.3 mM Na_3 GTP, pH 7.2 (290 mosmol/kg-H2O). In such conditions, the equilibrium potential for chloride ions (ECl) was −60 mV while the cations reverse potential (Ecat) was 0 mV. Signals were recorded using a Multiclamp 700B amplifier (Molecular Devices, San Jose, CA, USA). Signals were low-pass filtered (4 kHz), digitized (20 kHz) using a Digidata 1440A interface, and acquired online using pClamp 10 software (Molecular Devices, San Jose, CA, USA). Analyses were performed off-line using Axograph X.1.5.4 software (AxoGraph Scientific Software, Sydney, Australia). In voltage-clamp experiments, cells were recorded either at a holding potential of −60 or 0 mV to isolate cationic and chloride currents, respectively. Electrical stimulations of longitudinal axons located in the MZ were performed using bipolar platinum electrodes (FHC, Bowdoin, ME, USA) placed 500 μm rostrally to the recording site. Stimulations were performed at a low frequency (0.016 Hz) in order to evoke a stable response.

2.3 | Pharmacological agents

During patch-clamp recordings, all drugs were applied via the bath perfusion system. Typically, the effect of drugs reached a steady-state within 3–4 minutes after solution switch, and the mean recovery time was ~15 min. Activity was recorded for at least 5 min at steady state under each condition. The following pharmacological agents were used:

Acetylcholine chloride (100 μM, Sigma-Aldrich, Darmstadt, Germany), TTX (0.3–1 μM, Alomone Labs, Jerusalem, Israel), gabazine (3 μM, Tocris Bioscience, Minneapolis, MN, USA), (+)-Nicotine hydrogen tartrate salt (10 μM, Sigma-Aldrich, Darmstadt, Germany), QX-314-Cl (1 mM, Sigma-Aldrich, Darmstadt, Germany), CNQX Disodium (20 μM, Tocris Bioscience, Minneapolis, MN, USA), DL-APV (200 μM, Tocris Bioscience, Minneapolis, MN, USA), Mecamylamine hydrochloride (50 μM, Tocris Bioscience, Minneapolis, MN, USA), and D-tubocurarine chloride (5 μM, Tocris Bioscience, Minneapolis, MN, USA).

2.4 | Fetal nicotine exposure

8–12 weeks old gestating mice received from E10.5 to E14.5 either a chronic subcutaneous (s.c) infusion of a physiological saline (0.9% NaCl, Vehicle, $N = 10$) or nicotine in buffered saline solution (Nicotine-treated, $N = 14$; pH = 7.4) via mini-osmotic pumps (Alzet, Cupertino, CA, USA). Nicotine concentrations were calculated as the base. Nicotine hydrogen tartrate salt (Sigma-Aldrich, Darmstadt, Germany) was used to prepare stock solutions. The nicotine tartrate salt was dissolved in sterile, physiological saline and administered continuously in a volume of 10 mg/d/kg body weight

2.5 | Immunohistochemistry

For confocal microscopy, E12.5–E14.5 CNP-EGFP negative and positive embryos were collected from pregnant females. Embryos were immediately fixed by immersion in PBS containing 4% PFA (freshly prepared, pH 7.4) for 2 hr at 4°C. Embryos were then rinsed with PBS and cryoprotected in PBS containing 20% sucrose. Tissues were embedded in OCT medium (VWR, Fontenay-sous-bois, France) and quickly frozen at −50°C in isopentane. 50-μm-thick serial floating coronal sections were obtained using a cryostat (Leica, Wetzlar, Germany) and stored in PBS at 4°C. For immunostaining, sections were then washed in PBS and incubated for 1 hr in a blocking solution (1% fish gelatin in PBS) with 0.3% Triton X-100 and then for 48 hr at 4°C with the primary antibodies, which were diluted in the blocking solution containing 0.4% Triton X-100. Sections were then washed in PBS and incubated for 3 hr at room temperature in the secondary antibodies, diluted in 0.4% Triton X-100 blocking solution. After washing in PBS, slides were dried and mounted in Mowiol medium (Millipore, Darmstadt, Germany).

The following primary antibodies were used: a guinea pig polyclonal anti-NG2 antibody (kindly provided by William B. Stallcup, Burnham Institute for Medical Research, La Jolla, California), a rabbit polyclonal anti-Olig2 antibody (Millipore, Darmstadt, germany), a mouse monoclonal anti-Ki-67 antibody (BD Pharmigen, Franklin Lakes, NJ, USA), a mouse monoclonal anti-nestin antibody (Millipore), a rabbit polyclonal anti-VIAAT antibody (Dumoulin et al., 1999; kindly provided by Bruno Gasnier, Neurophotonics Lab, Université Paris Diderot, Paris, France) and a rabbit polyclonal anti-VGluT2 antibody (Herzog et al., 2001; kindly provided by S. El Mestikawy, Laboratoire Neuroscience Paris Since, Université Pierre et Marie Curie, Paris). Alexa Fluor 405-, or 594- and 647-conjugated secondary antibodies (1/500; Invitrogen, Waltham, MA, USA) were used to detect mouse monoclonal, guinea pig and rabbit polyclonal.

2.6 | Confocal microscopy

Immunostainings were imaged using a SP5 confocal microscope (Leica, Darmstadt, Germany) using a 20× oil-immersion objective with a numerical aperture of 1.25, as well as with a 63× oil-immersion objective with a numerical aperture of 1.32 and a 1× digital zoom magnification. Serial optical sections were obtained with a Z-step of 4 μm (20×) and 2 μm (63×). Images (1024 × 1024; 8-bit grayscale) were stored using Leica software LAS-AF and analyzed using ImageJ 1.41 (National Institutes of Health; http://rsb.info.nih.gov/ij/) and Adobe Photoshop CS6 (Adobe software, San Jose, CA, USA). Quantifications were performed manually on 20-μm-thick transverse sections using ImageJ software.

2.7 | Electron microscopy

Synapse formation onto nestin-positive cells was analyzed by the pre-embedding immunogold method with silver-enhancement (Bernard, Levey, & Bloch, 1999). 2 mm-thick sections were made at the hindlimb level of E12.5 embryos and were immersion-fixed in PB with 0.2% glutaraldehyde and 2% paraformaldehyde (PFA) at room temperature during 1 hr and further post-fixed in PB with 2% PFA at 4°C during 1 hr. After agarose inclusion, 80 μm-thick vibratome coronal sections were immunolabeled with a mouse monoclonal anti-Nestin antibody (Millipore, Darmstadt, Germany) and an anti-mouse biotinylated antibody and Nanogold streptavidine (Nanoprobes, Yaphank, NY, USA). The diameter of gold particles was increased using a silver enhancement (HQ silver, Nanoprobes, Yaphank, NY, USA). Sections were then post-fixed, dehydrated and embedded in epon resin. Areas of interest were cut and glued onto resin blocks. 70 nm-thick sections were cut with an ultracut UCT microtome (Leica, Wetzlar, Germany), stained with lead citrate and Uranyless (Delta Microscopies, Mauressac, France) and analyzed with a transmission electron microscope (EM 912 Omega, Zeiss, Oberkochen, Germany). Images were captured with a digital camera (SS-CCD, Proscan 1kx1k, Toronto, Canada) and analyzed with the iTEM software.

2.8 | Data analysis

Standard off-line detection of synaptic currents was done with Axograph X.1.5.4 software (AxoGraph Scientific Software, Sydney, Australia). In brief, a template was generated and used to scan the raw trace for similar waveforms. All matching events were stored and, when present, false positive events were discarded, either manually or automatically on the basis of their amplitude or kinetics. Mean synaptic currents rate was then calculated every second and plotted in 30 s binning over the whole time course of the experiments. For the quantification of the mean effects of acetylcholine and nicotine, the mean rates were calculated at the steady state for 4–6 min as indicated in the results section.

2.9 | Statistics

All values are expressed in the text as mean ± *SEM*. For data sets with multiple conditions ($N > 2$), the data set was first subjected to a Kruskal-Wallis one-way analysis of variance followed by Dunn's multiple comparison test. For data set comprising only two conditions, a Mann-

Whitney non-parametric *U* test was used for unpaired data points or a Wilcoxon signed ranked test *R* for paired data points. $p < .05$ and $p < .01$ were taken respectively as significant and highly significant.

3 | RESULTS

3.1 | Pioneer OPCs accumulate preferentially in the ventro-lateral domain of the marginal zone surrounding the motor exit point

In the mouse spinal cord, the first wave of OPCs is generated between E12 and E14 from olig2-expressing neuroepithelial precursors forming the pMN domain (Bergles & Richardson, 2016). While it is known that these pioneer OPCs first colonize the ventral half of the spinal cord, their exact location, morphology and density during this process remain poorly characterized. To address this issue, we performed immunostaining for NG2 and Olig2 onto coronal sections of spinal cord between E11.5 and E14.5.

At E11.5, we did not observe any NG2 immunoreactivity in the olig2$^+$ pMN domain, although pericytes lining capillaries were already intensely labelled for NG2 (data not shown). At E12.5, NG2 started labeling a subpopulation of cells in the olig2-expressing VZ domain (Figure 1a1,a2). At this stage, only few NG2$^+$/Olig2$^+$ somas could be found outside the pMN domain in the ventral parenchyma and none in the MZ. However, we observed numerous NG2-positive glial processes running through the parenchyma and into the MZ to contact the basal lamina (Figures 1a3 and 2). These NG2-positive glial processes were more abundant around the motor exit point (MEP), where cholinergic MN axons exit the spinal cord (Figures 1a3 and 2). Discrete spots of NG2 immunoreactivity could also be observed lining the central canal, suggesting that the first OPCs generated by the pMN domain exhibit a radial morphology—that is with radial processes contacting the basal lamina as well as the central canal. Because these morphological features were reminiscent of neuroepithelial precursors, also known as radial glial cells at this developmental stage, we performed co-immunostaining for NG2 and Nestin, a marker of neuroepithelial precursors (Figure 2). We found a high degree of co-localization between NG2 and Nestin in glial processes located in the MZ around the MEP, suggesting a subset of neuroepithelial precursors transiently co-express Nestin and NG2 as they start differentiating into OPCs at E12.5.

Accordingly, we also observed a high degree of co-localization between NG2 and GLAST, a transmembrane glutamate astrocyte transporter known to be expressed in the membrane of neuroepithelial precursors at this developmental stage (Figure 2c; Barry, Pakan, O'Keeffe, & McDermott, 2013; Shibata et al., 1997).

At E13.5, numerous NG2$^+$/Olig2$^+$ cells were observed in the pMN domain (Figure 1b1,b2,e3) but very few at E14.5 (Figure 1c1,c2, e3). These results confirmed that the emergence of pioneer OPCs from their neuro-epithelial precursors in the pMN domain is restricted to a short time window starting at E12.5 and tapering at E14.5.

After they leave the pMN domain, pioneer NG2$^+$/Olig2$^+$ cell bodies started colonizing the ventral parenchyma and the MZ around E13.5. At E14.5, they were found preferentially accumulating around the MEP where the highest density of NG2-positive glial endfeet was previously observed at E12.5 (Figures 1a3 and 2). Indeed, the density of NG2$^+$/Olig2$^+$ cells was significantly higher in the part of the MZ surrounding the MEP compared with any other areas of the embryonic spinal cord (Figure 1e2). Taken together, these observations suggest a particular affinity of pioneer OPCs for the MZ surrounding the MEP. This area is known to contain cholinergic MN axons and dendrites as well as longitudinal axons from GABAergic and glutamatergic premotor INs (Czarnecki et al., 2014; Vaughn et al., 1974). We previously showed that premotor INs initiate synaptogenesis in the spinal cord by forming the first synapses onto MNs between E12.5 and E13.5 in the MZ (Czarnecki et al., 2014; Scain et al., 2010).

3.2 | Pioneer OPCs receive functional glutamatergic and GABAergic axoglial synapses

To determine whether axoglial synapses could also be formed onto pioneer OPCs in the MZ, we first performed co-immunostainings for NG2 with either VGluT2 or VIAAT, which stain putative vesicular release sites for glutamate and GABA/Glycine vesicular transporters, respectively (Figure 3). Immunostainings were performed using CNP-EGFP mouse embryos to easily discriminate NG2$^+$/CNP-EGFP$^+$ OPCs from NG2$^+$/CNP-EGFP$^-$ pericytes. In these mice, MNs exhibited a low level of EGFP expression, a likely consequence of the expression of EGFP in the pMN domain at earlier developmental stages. As previously described (Czarnecki et al., 2014), we first confirmed that VGluT2 and VIAAT-immunoreactive aggregates were mostly restricted to the MZ. Both VIAAT and VGLUT2 aggregates could be found apposing to NG2+/CNP-EGFP$^+$ processes and cell bodies (Figure 3), suggesting that vesicular synaptic release of GABA and glutamate may indeed occur from longitudinal axons to OPC processes and cell bodies located in the MZ.

To determine whether these putative synaptic contacts were functional, we performed whole-cell patch-clamp recordings of EGFP$^+$ cells located in the MZ using whole spinal cord preparations obtained from E13.5 and E14.5 CNP-EGFP mouse embryos. Virtually all EGFP$^+$ cells located in the MZ were found positive for NG2 and Olig2 immunolabeling (Figure 4C). To further confirm that CNP-EGFP$^+$ cells recorded in the MZ were OPCs, we filled some of them with biocytin through the patch pipette and performed post-hoc staining for NG2. All biocytin-filled CNP-EGFP$^+$ cells were found positive for NG2 immunolabeling (6/6 cells). They exhibited an elongated morphology along the longitudinal axis with their processes aligned to funicular axons, a morphological feature typical of OPCs found in axon tracts (Figure 4). Recorded EGFP$^+$ cells had an average capacitance of 10.2 ± 2.6 pF ($N = 40$) and an average input resistance of 1.81 ± 0.44 GΩ ($N = 40$). Recorded cells displayed significant voltage-gated outward K$^+$ currents but little or no voltage-gated inward Na$^+$ currents, as expected for OPCs (Figure 4). Recorded cells were unable to fire action potentials when recorded in current-clamp mode (data not shown).

When the membrane potential (Vh) was equal to the chloride equilibrium potential (ECl = -60 mV; see Section 2), recordings of spontaneous activity revealed the presence of fast inwards currents having an average amplitude of -7.5 ± 0.7 pA, a 20%–80% rise time of 0.293 ± 0.02 ms and a decay time constant of 1.33 ± 0.13 ms
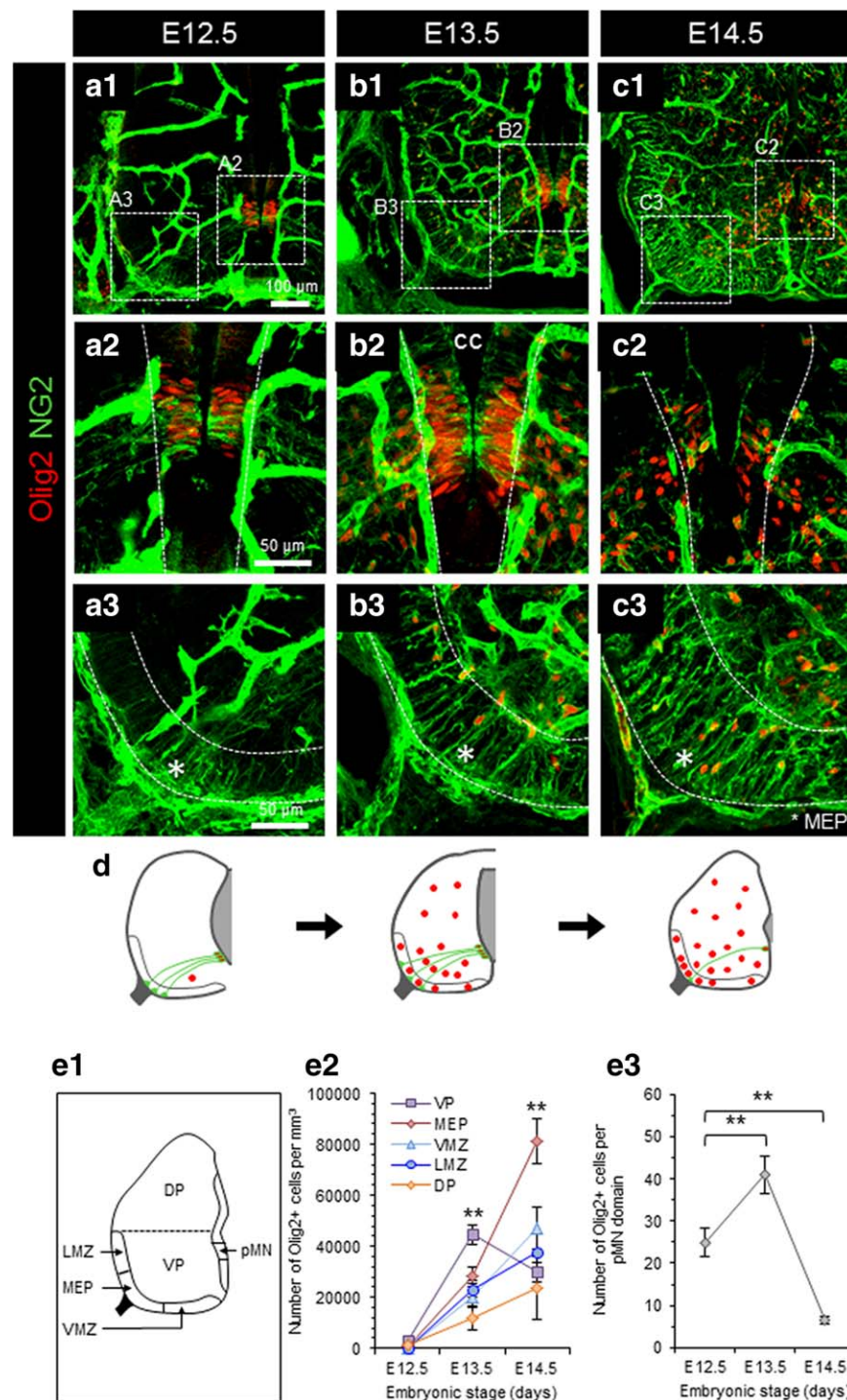
FIGURE 1 Pioneer OPCs preferentially accumulate in the marginal zone surrounding the motor neuron axon exit point. (a1–c1) Confocal images showing immunofluorescence stainings for Olig2 (red) and NG2 (green) in coronal sections of mouse spinal cord at E12.5, E13.5, and E14.5. The most intense NG2 staining corresponds to the pericytes lining blood vessels. (a2–c2) Olig2 cells in the pMN domain start expressing the proteoglycan NG2 at E12.5. Two days later at E14.5, only few NG2$^+$/Olig2$^+$ cells are still present in the pMN domain. Dotted lines mark the limit between the ventricular zone and the parenchyma. (a3–c3) radial processes labelled by NG2 are first observed in the marginal zone surrounding the motor exit point (MEP, marked by the asterisk) at E12.5 while the first NG2$^+$/Olig2$^+$ soma only reach the MEP at E13.5, where they preferentially accumulate. Dotted lines mark the outer and inner limits of the marginal zone. (d) Drawings summarizing the location of NG2 positive radial processes (in green) and Olig2 somas (in red) at E12.5, E13.5, and E14.5 in the spinal cord. (e1) Schematic figure illustrating the different areas quantified in e2 and e3. (e2) Quantifications of the density of Olig2 positive cells in different location of the ventral spinal cord at E12.5, E13.5, and E14.5. Note the preferential accumulation of Olig2 cells in the MEP at E14.5. (e3) quantifications of the number of Olig2 cells observed in the pMN domain per section. ($N = 8$–12 per embryonic stage). Data are represented as mean $\pm$ *SEM*. Statistical difference for the density (e2) and number (e3) of Olig2-immunopositive cells in the MEP and pMN domain, respectively, are indicated (*$p < .05$, **$p < .01$). LMZ = lateral marginal zone; MEP = motor exit point; VMZ = ventral marginal zone; VP = ventral parenchyma; DP = dorsal parenchyma; pMN = precursor of motoneuron domain [Color figure can be viewed at wileyonlinelibrary.com]
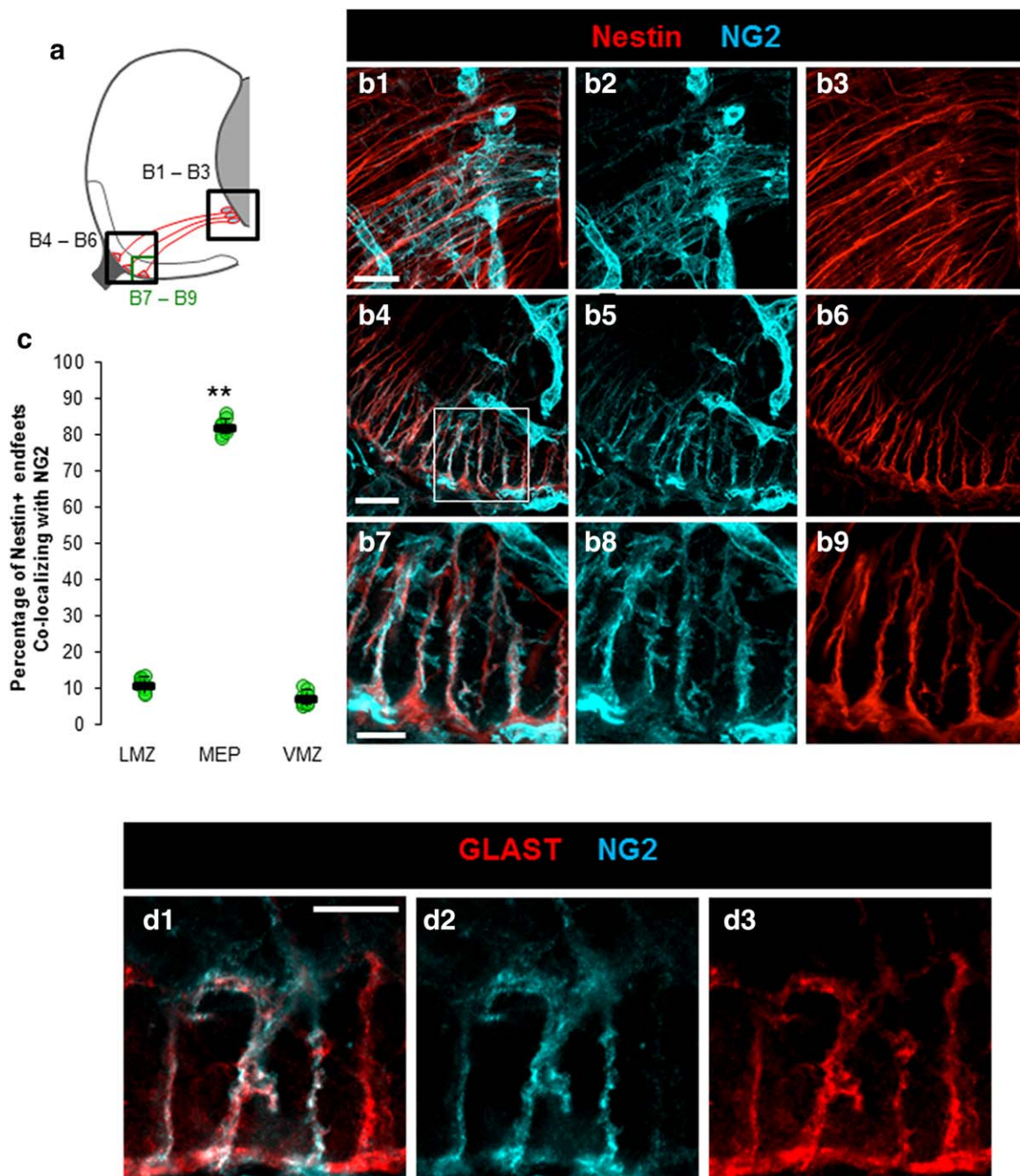
FIGURE 2 NG2 immunostaining is detected in nestin-positive radial glia endfeet at E12.5 in the marginal zone. (a) Drawing showing where the confocal images were taken in the spinal cord in b. (b1–b9) Confocal images showing immunofluorescence stainings for Nestin (red) and NG2 (cyan) in coronal sections of E12.5 mouse spinal cord. NG2 staining was found to colocalize both with nestin-positive processes in the pMN domain contacting the central canal (b1–b3), in nestin-positive processes found across the parenchyma (b4–b6) and in nestin-positive endfeet contacting the marginal zone surrounding the motor exit point (b7–b9). Scale bars represent 20 μm in b1–b6 and 10 μm in b7–b9. (c) Plot quantifying the percentage of NG2$^+$/Nestin$^+$ endfeet located in the lateral marginal zone (LZ), around the motor exit point (MEP) and in the lateral and ventral marginal zone ($N = 5$ embryos). Statistical differences are as indicated (**$p < .01$). (d1–d3) Confocal images showing immunofluorescence stainings for GLAST (red) and NG2 (cyan) in coronal sections of E12.5 mouse spinal cord. Note how NG2 staining colocalize with GLAST in glial endfeet surrounding the motor exit point. Scale bar represents 10 μm [Color figure can be viewed at wileyonlinelibrary.com]

($N = 25$) consistent with previous reports of glutamatergic spontaneous postsynaptic currents (sPSC) in OPCs at postnatal developmental stages (Bergles & Richardson, 2016; Figure 5a). sPSC were fully blocked by the superfusion of 200 μM DL-APV and 10 μM CNQX ($N = 11$) as well as by CNQX alone ($N = 9$), indicating that they were mediated by AMPA/

kainate glutamate receptors (Figure 5a1,a2). Inward sPSC had an average frequency of 0.043 ± 0.010 Hz and were almost completely blocked by TTX superfusion (1 μM; $-99.61\% \pm 1.22\%$, $p < .01$) indicating that they are dependent on neuronal action potential (AP) firing (Figure 9a5). Moreover, direct electrical stimulation of funicular axons was found to elicit
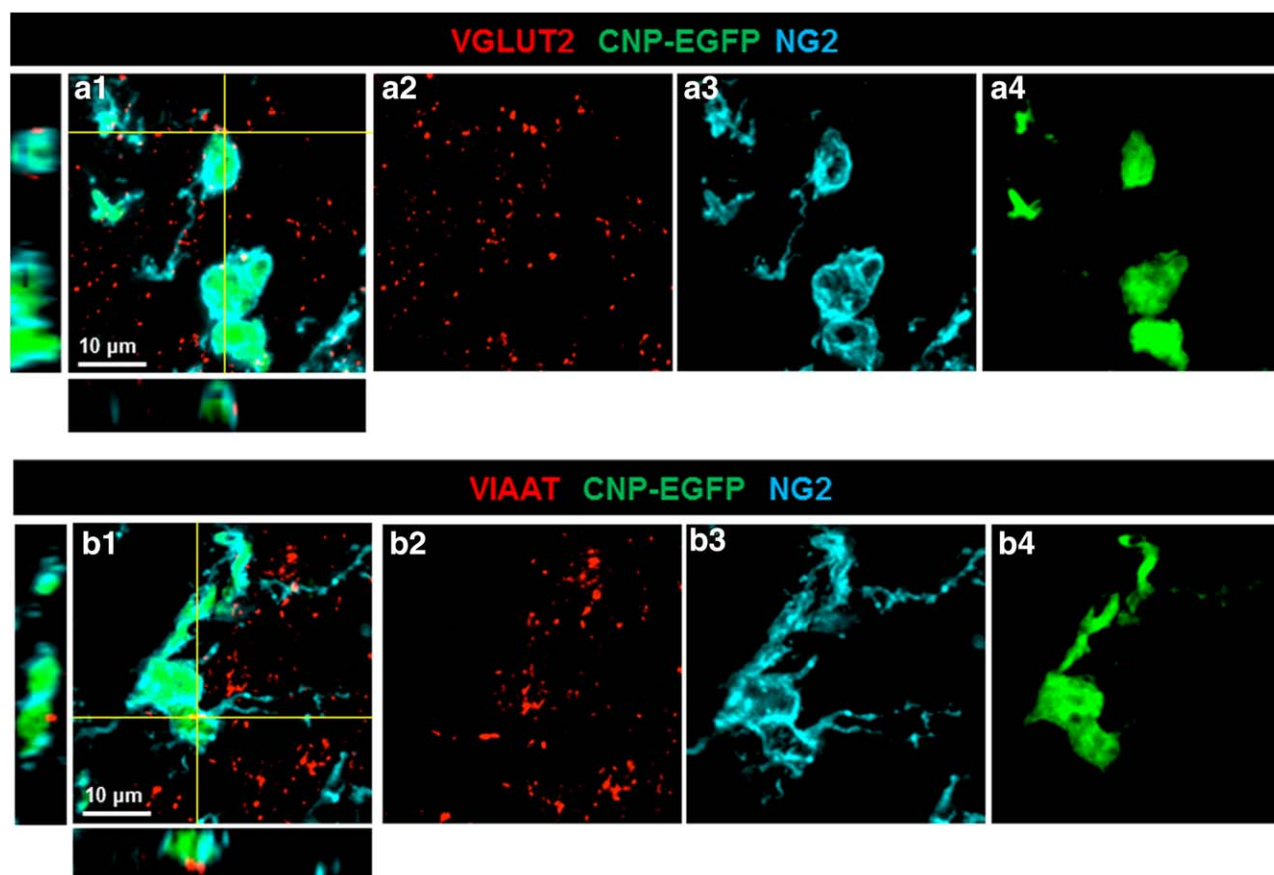
FIGURE 3 Putative release sites for glutamate and GABA are found apposed to OPCs located in the MEP. (a1–a4) High magnification confocal images showing the apposition of vesicular glutamate transporter, VGluT2$^+$ puncta (red) to pioneer OPCs located in the MEP and identified by their expression of CNP-EGFP (in green) and NG2 (in cyan) in coronal sections of CNP-EGFP mouse spinal cord at E14.5. (b1–b4) High magnification confocal images showing the apposition of the vesicular inhibitory amino acid transporter, VIAAT$^+$ puncta (in red) to pioneer OPCs located in the MEP and identified by their expression of CNP-EGFP (in green) and NG2 (in cyan) in coronal sections of CNP-EGFP mouse spinal cord at E14.5. Scale bars = 10 μm [Color figure can be viewed at wileyonlinelibrary.com]

ephaptic-like currents—resulting from compound AP in funicular axons (Jefferys, 1995)—followed by fast-rising inward currents with an average amplitude of −35.7 ± 10.8 pA (N = 8; Figure 6a,b). Fast-rising inward currents were fully blocked by superfusion of DL-APV and CNQX (N = 8) as well as by CNQX alone (N = 9). Taken together, our results demonstrate the existence of functional synapses between longitudinal glutamatergic axons located in the MZ and OPCs, at least as early as E13.5.

To assess the presence of GABA/glycine postsynaptic currents, we recorded OPC at a holding potential of 0 mV, the cationic equilibrium potential in our experimental conditions (Figure 5b). In this configuration, OPCs displayed spontaneous outward currents with an average amplitude of 4.4 ± 0.7 pA, a rise time (20%–80%) of 1.81 ± 0.15 ms and a decay time constant of 86.75 ± 10.21 ms (N = 10; Figure 5b). Superfusion of the GABA$_A$R selective antagonist Gabazine (10 μM) fully blocked these outward sPSC (N = 6; Figure 5b1,b2) confirming that they were GABAergic events. Outward sPSCs had an average frequency of 0.017 ± 0.003 Hz and were almost completely blocked by TTX superfusion (1 μM; −98.27% ± 5.19%, p < .01; N = 9; Figure 9b5). Finally, direct electrical stimulation of funicular axons was found to elicit slow rising outward currents with an average amplitude of 10.1 ± 2.8 pA (N = 9) that were also blocked by superfusion of

gabazine (N = 6; Figure 6d,e). These results indicate that, in addition to glutamatergic synapses, functional GABAergic axoglial synapses are also formed between GABAergic axons located in the MZ and pioneer OPCs as soon as E13.5.

Finally, to determine whether such axoglial synapses are formed onto the radial processes of neuro-epithelial precursors as they start differentiating into OPCs, we investigated the presence of axoglial synapses onto nestin-positive processes located around the MEP at E12.5. Indeed, we found that most nestin-positive processes located in the MEP appear to co-express the proteoglycan NG2 at this stage (Figure 2). Strikingly, electron microscopy revealed the presence of synaptic-like axoglial contacts onto nestin-positive endfeet located in the MEP (Figure 7). These observations indicate that axoglial synapses could already be forming onto the endfeet of neuro-epithelial precursors as they commit to an OPC fate.

3.3 | GABAergic and glutamatergic axoglial synapses are potentiated by the activation of presynaptic nicotinic acetylcholine receptors

Because pioneer OPCs tend to accumulate around the MEP, we investigated the possible influence of cholinergic signaling from MN
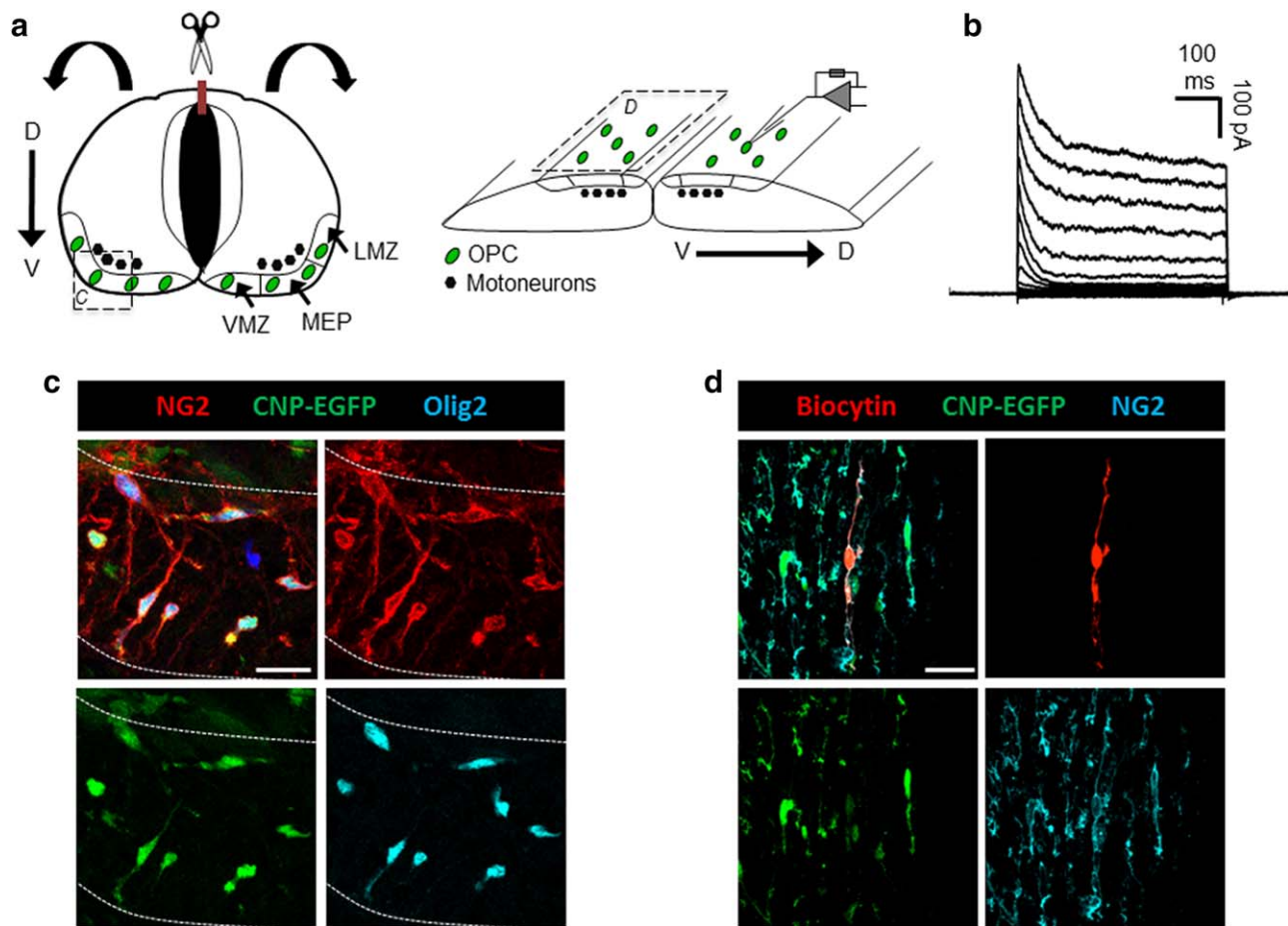
FIGURE 4 CNP-GFP$^+$ cells located in the marginal zone exhibit typical electrophysiological properties of OPCs. (a) Drawing of the "open-book" whole spinal cord preparation obtained from CNP-EGFP mouse embryo SC to record pioneer OPCs in the spinal cord. (b) Representative responses in voltage-clamp to voltage steps (a, −100 to −10 mV, step size 10 mV) of a NG2$^+$/EGFP$^+$ pioneer OPC located at the MEP in a E13.5 CNP-EGFP mouse embryo. Note the presence of both transient IK$_A$ and sustained IK$_{DR}$ outward current in response to depolarizing voltage steps. (c) Confocal image showing immunofluorescence stainings for NG2 (red) and olig2 (cyan) in the MEP of a CNP-EGFP (Green) mouse embryo at E13.5. Note how CNP-EGFP cells located in the MEP are also immuno-positive for NG2 and Olig2. Dotted lines mark the outer and inner limits of the marginal zone. Scale bar = 20 μm. (d) Confocal images from a whole spinal cord preparation showing the cell recorded in b filled with biocytin (in red) and co-expressing CNP-EGFP (in green) and NG2 (in cyan). Note how NG2$^+$/CNP-EGFP$^+$ cell processes tend to be longitudinally aligned along the antero-posterior axis. Scale bar = 20 μm [Color figure can be viewed at wileyonlinelibrary.com]

onto OPCs. Immunostainings for the vesicular acetylcholine transporter vAChT labeled numerous putative release sites around MN soma and inside the MZ, localized specifically around the MEP (Figure 8). Strikingly, many of these vAChT-positive puncta in the MEP were found in the direct vicinity of NG2$^+$/CNP-EGFP$^+$ soma and processes, supporting the hypothesis that pioneer OPCs around the MEP could be influenced by acetylcholine released from MNs.

To address this possibility, we investigated the effect of acetylcholine application onto OPCs by patch-clamp recordings. Acetylcholine application (100 μM) did not induce any significant change in baseline current in any of the recorded OPCs ($N = 10$), suggesting that AchR are not functional or are not expressed by pioneer OPCs in the embryonic spinal cord. In contrast, we observed that the same application of acetylcholine significantly increased the frequency of both glutamatergic and GABAergic spontaneous PSCs (Figure 9a2,b2). Acetylcholine had no significant effect on the average amplitude of glutamatergic (control:

−10.1 ± 2.2 pA vs. Ach: −9.1 ± 1.9 pA, $N = 10$) and GABAergic (control: 5.35 ± 1.6 pA vs. Ach: 4.9 ± 1.5 pA, $N = 7$) spontaneous PSCs. The action of acetylcholine on the frequency of glutamatergic and GABAergic spontaneous PSC was blocked by the co-superfusion of mecamylamine (50 μM) and d-tubocurarine (5 μM; Figure 9a3,b3). Mecamylamine is a non-competitive nicotinic acetylcholine receptor antagonist (Arias et al., 2010) and D-Tubocurarine is a classical non-selective nAChR antagonist (Jonsson et al., 2006). It has been previously shown that the combination of these two antagonists is necessary and sufficient in order to suppress cholinergic transmission in the embryonic mouse spinal cord (Hanson & Landmesser, 2003). The effect of acetylcholine application on the frequency of glutamatergic and GABAergic PSCs could be mimicked by the application of nicotine (10 μM; Figures 9a4, b4). Nicotine had no effect on the average amplitude of glutamatergic (control: −7.9 ± 1.4 pA vs. nicotine: −8.1 ± 1.6 pA, $N = 8$) and GABAergic (control: 4.2 ± 1.4 pA vs. nicotine: 4.4 ± 1.4 pA, $N = 10$) spontaneous
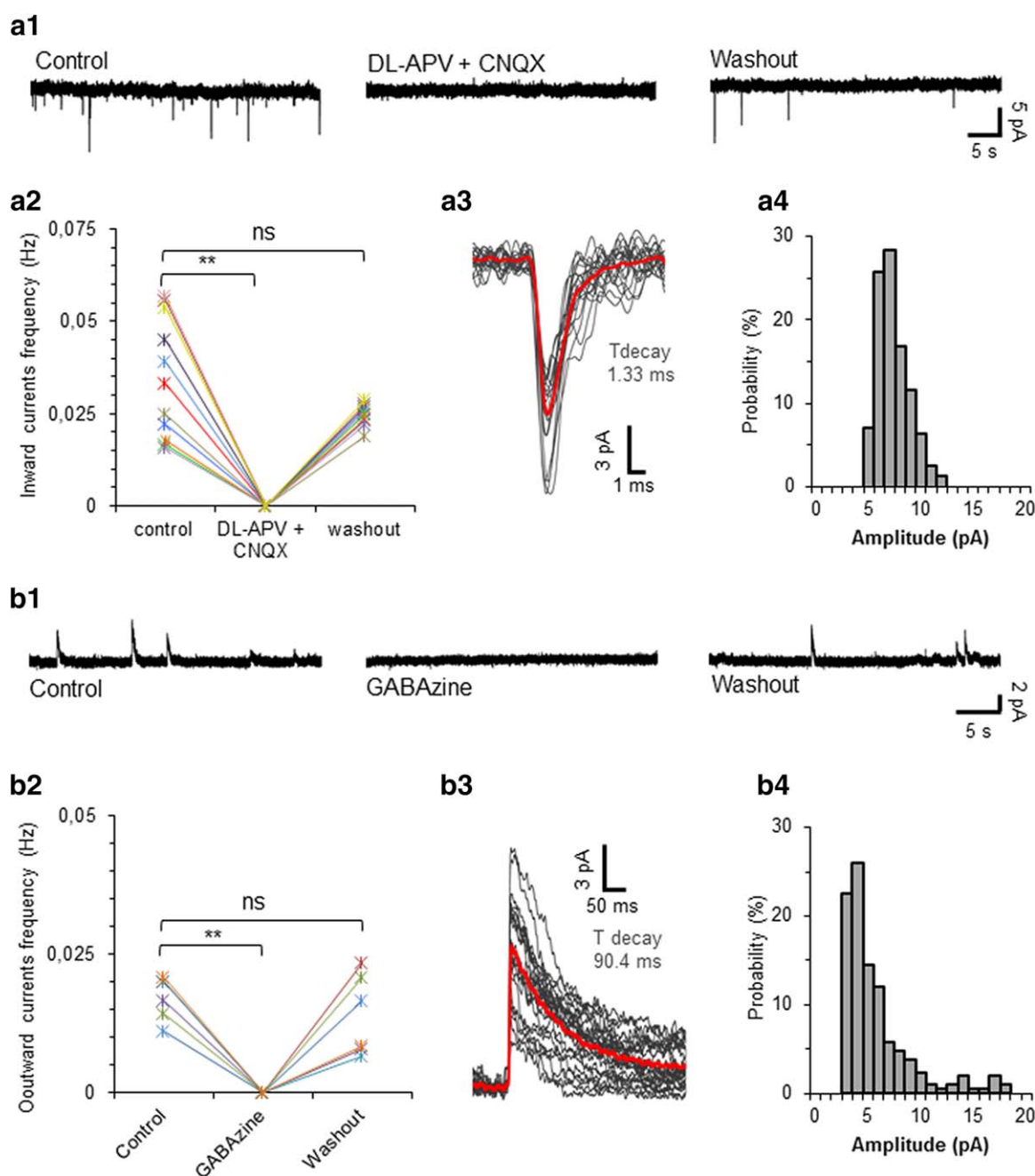
FIGURE 5   Pioneer OPCs are already contacted by functional glutamatergic and GABAergic axoglial synapses when their somas reach the MZ. (a1) Representative voltage-clamp recordings from a CNP-EGFP$^+$ OPC located in the MEP at E13.5. At a holding potential of −60 mV, the cell exhibited fast inward currents (left trace, control) that were blocked by the application of AMPAR/KAR and NMDAR antagonists (center trace, DL-APV 200 μM/CNQX 20 μM) in a reversible manner (right trace, washout). (a2) Summary plot quantifying the partially reversible blockade of fast inward currents by DL-APV and CNQX ($N = 11$; **$p < .01$, paired student t test). (a3) Example traces showing the kinetic of individual inward currents (in black) and their average (in red) recorded from the same OPC as in a1. These inward currents exhibited an average mono-exponential decay time constant of 1.33 ms, as expected from synaptic currents mediated by AMPA/KA receptors. (a4) Plot showing the distribution of fast inward current amplitudes. (b1) Representative voltage-clamp recordings from another CNP-EGFP$^+$ OPC located in the MEP at E13.5. At a holding potential of 0 mV, the cell exhibited slow outward currents (left trace, control) that were blocked by the application of a GABA$_A$R antagonist (center trace, gabazine 10 μM) in a reversible manner (right trace). (b2) Summary plot quantifying the partially reversible blockade slow outward currents by gabazine ($N = 6$; **$p < .01$). (b3) Example traces showing the kinetic of individual outward currents (in black) and their average (in red) recorded from the same OPC as in b1. These inward currents exhibited an average mono-exponential decay time constant of 90.4 ms, as expected from synaptic currents mediated by GABA$_A$R receptors. (b4) Plot showing the distribution of slow outward current amplitudes [Color figure can be viewed at wileyonlinelibrary.com]
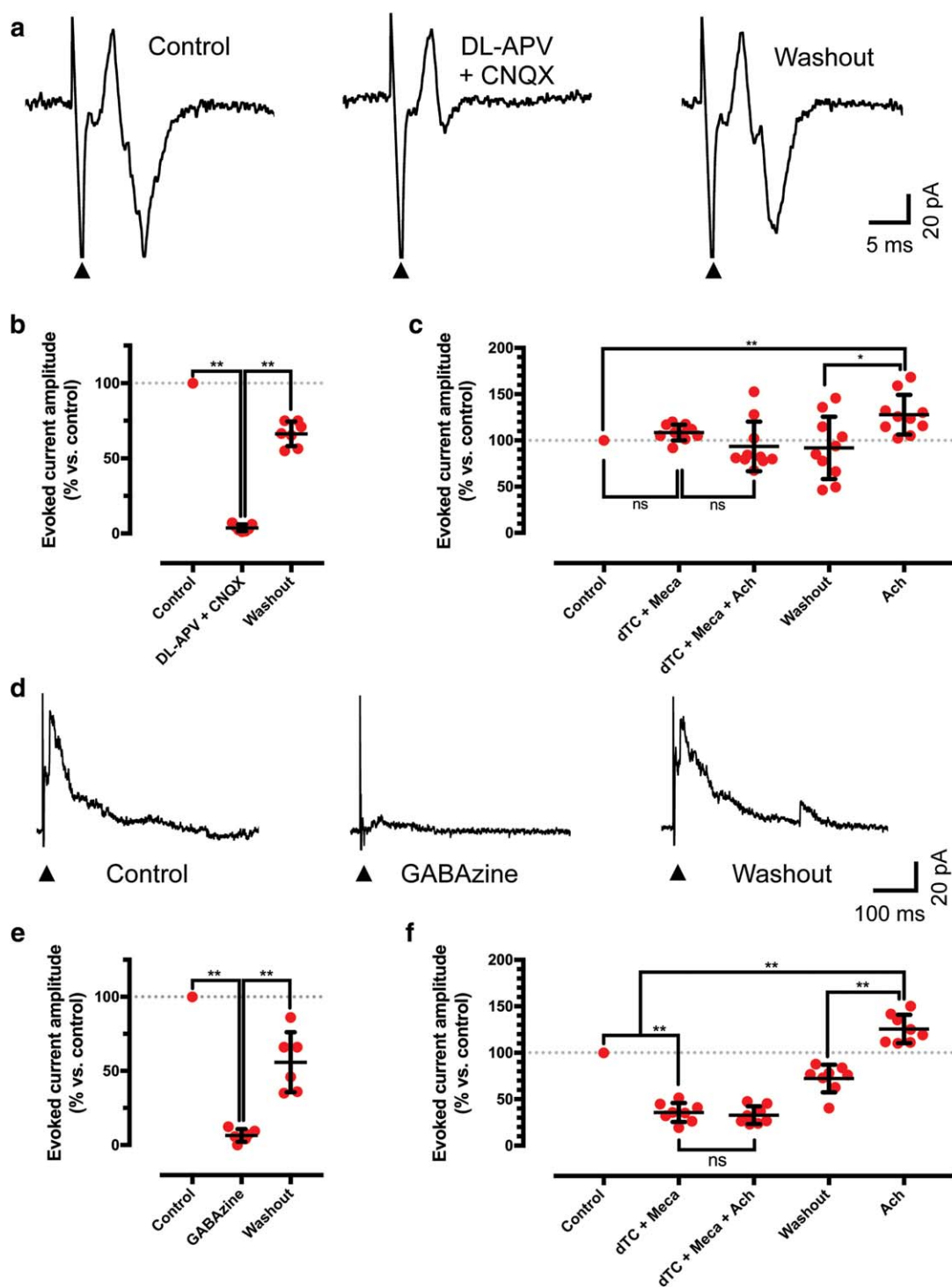
FIGURE 6 Cholinergic signaling potentiates glutamatergic and GABAergic synaptic currents evoked in OPCs by electrical stimulation of the marginal zone. (a) Representative voltage-clamp recordings from a CNP-EGFP⁺ OPC located in the MEP at E13.5. At a holding potential of −60 mV, electrical stimulation of the marginal zone evoked inward currents (left trace, control) that were blocked by the application of AMPAR/KAR and NMDAR antagonists (center trace, DL-APV 200 μM/CNQX 20 μM) in a reversible manner (right trace, washout). (b) Summary plot quantifying the partially reversible blockade of fast inward currents by DL-APV and CNQX ($N = 9$; **$p < .01$). (c) Plots summarizing the effects of various manipulations of cholinergic signaling on the amplitude of glutamatergic synaptic currents evoked in pioneer OPCs by electrical stimulation of the marginal zone. Statistical differences (**$p < .01$, paired student t test) are shown. (d) Representative voltage-clamp recordings from a CNP-EGFP⁺ OPC located in the MEP at E13.5. At a holding potential of 0 mV, electrical stimulation of the marginal zone evoked outward currents (left trace, control) that were blocked by the application of GABA_ARs antagonists (center trace, Gabazine 10 μM) in a reversible manner (right trace, washout). (e) Summary plot quantifying the partially reversible blockade of slow outward inward currents by gabazine ($N = 6$; **$p < .01$). (f) Plots summarizing the effects of various manipulations of cholinergic signaling on the amplitude of GABAergic synaptic currents evoked in pioneer OPCs by electrical stimulation of the marginal zone. Statistical differences (**$p < .01$, paired student t test) are shown [Color figure can be viewed at wileyonlinelibrary.com]
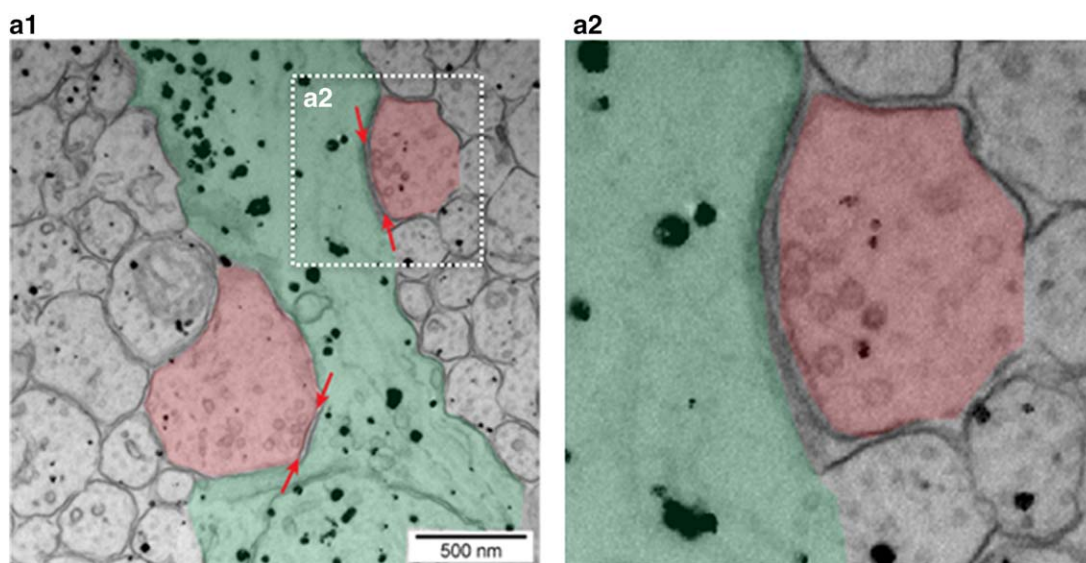
FIGURE 7 Neuro-epithelial precursors receive synaptic-like axoglial contacts onto their endfeet in the marginal zone. (a1 and a2) Electron micrographs showing a nestin-positive glial process located in the MEP (Silver intensified immunostaining, pseudo-colored in green) contacted by two synaptic-like axoglial contacts (pseudo-colored in red). The red arrows delimit the extent of the putative active zone where presynaptic vesicles can be observed. a2 show a magnified view of the putative axo-glial synapse located in the white dashed box in a1 [Color figure can be viewed at wileyonlinelibrary.com]

PSCs. Together, these results demonstrate that the effect of acetylcholine on PSC frequency is dependent on the activation of nicotinic AChRs (nAChR).

We found that the ability of nicotine to potentiate the frequency of both GABAergic and glutamatergic PSC was preserved in the presence of TTX (1 μM; Figure 9a5,b5), showing that nicotine and acetylcholine can promote PSC frequency by acting onto nAChR expressed by the presynaptic terminals of axoglial synapses. The amplitude of miniature glutamatergic PSCs (-7.6 ± 0.7 pA, $N = 9$) and miniature GABAergic PSCs (5.9 ± 0.7 pA, $N = 8$) observed during nicotine application were not significantly different from the amplitude of spontaneous glutamatergic PSCs (-7.8 ± 1.3 pA) and spontaneous GABAergic PSCs (6.0 ± 0.5 pA) recorded in control conditions in the same cells. To test whether endogenous source of acetylcholine could therefore participate to potentiate axoglial transmission onto OPC, we investigated the influence of nAChR antagonists onto sPSCs (Figures 9a3,a7,b3,b7) and onto PSCs evoked by direct electrical stimulation of funicular axons (Figure 6c,f). We found that the co-superfusion of mecamylamine (50 μM) and d-tubocurarine (5 μM) had little influence on glutamatergic sPSC frequency (Figure 9a3,a7) and on the amplitude of evoked glutamatergic PSCs (Figure 6c). By contrast, co-superfusion of mecamylamine (50 μM) and d-tubocurarine (5 μM) significantly decreased GABAergic sPSC frequency (Figure 9b3,b7) as well as the amplitude of evoked GABAergic PSCs (Figure 6f), thus indicating that endogenous cholinergic signaling act preferentially onto GABAergic axoglial synapses.

3.4 | Fetal nicotine exposure increases the density and proliferation of pioneer OPC in the ventral spinal cord

Our results show that exogenous nicotine has a significant effect on both glutamatergic and GABAergic axoglial transmission in pioneer OPCs found in the MZ (Figures 6 and 9). As nicotine readily cross the

placenta to reach the embryo (Ross, Graham, Money, & Stanwood, 2015), we investigated whether fetal exposure to nicotine could influence pioneer OPC density and proliferation as they emerge from the pMN domain and start colonizing the spinal cord.

At E10.5, we implanted gestating mice with osmotic pumps filled either with saline (Vehicle group, $N = 5$) or 10 mg/d/kg of nicotine (nicotine-treated group, $N = 6$). Doses of nicotine were chosen to reach a level in the circulating bloodstream of the pregnant female equivalent to moderately smoking pregnant women (Matta et al., 2007). To assess the distribution and proliferation rate of pioneer OPCs, we quantified the number of cells expressing Olig2$^+$ cells and Olig2$^+$/Ki67$^+$ in different parts of the MZ, in the ventral parenchyma, and in the dorsal parenchyma of E14.5 embryos treated with either saline or nicotine (Figure 10a). We found that nicotine increased the density of Olig2$^+$ cells in the MZ surrounding the MEP and in the ventral parenchyma by twofold compared with saline-treated embryos (Figure 10b). By contrast, density of Olig2$^+$ cells did not appear to be affected in the lateral and ventral part of the marginal zone, nor in the dorsal parenchyma. Moreover, we found that chronic nicotine treatment significantly increased the percentage of Olig2$^+$ cells co-expressing Ki67 around the MEP by twofold compared with saline-treated embryos (Figure 10c). Taken together, our results show that chronic nicotine treatment during gliogenesis preferentially increases the density and proliferation of OPC located in the MZ surrounding the MEP.

4 | DISCUSSION

In this study, we demonstrate that functional glutamatergic and GABAergic axoglial synapses are formed onto pioneer OPCs at least as soon as their soma reach the marginal zone—that is the area where synaptogenesis begins in the embryonic spinal cord. We found that
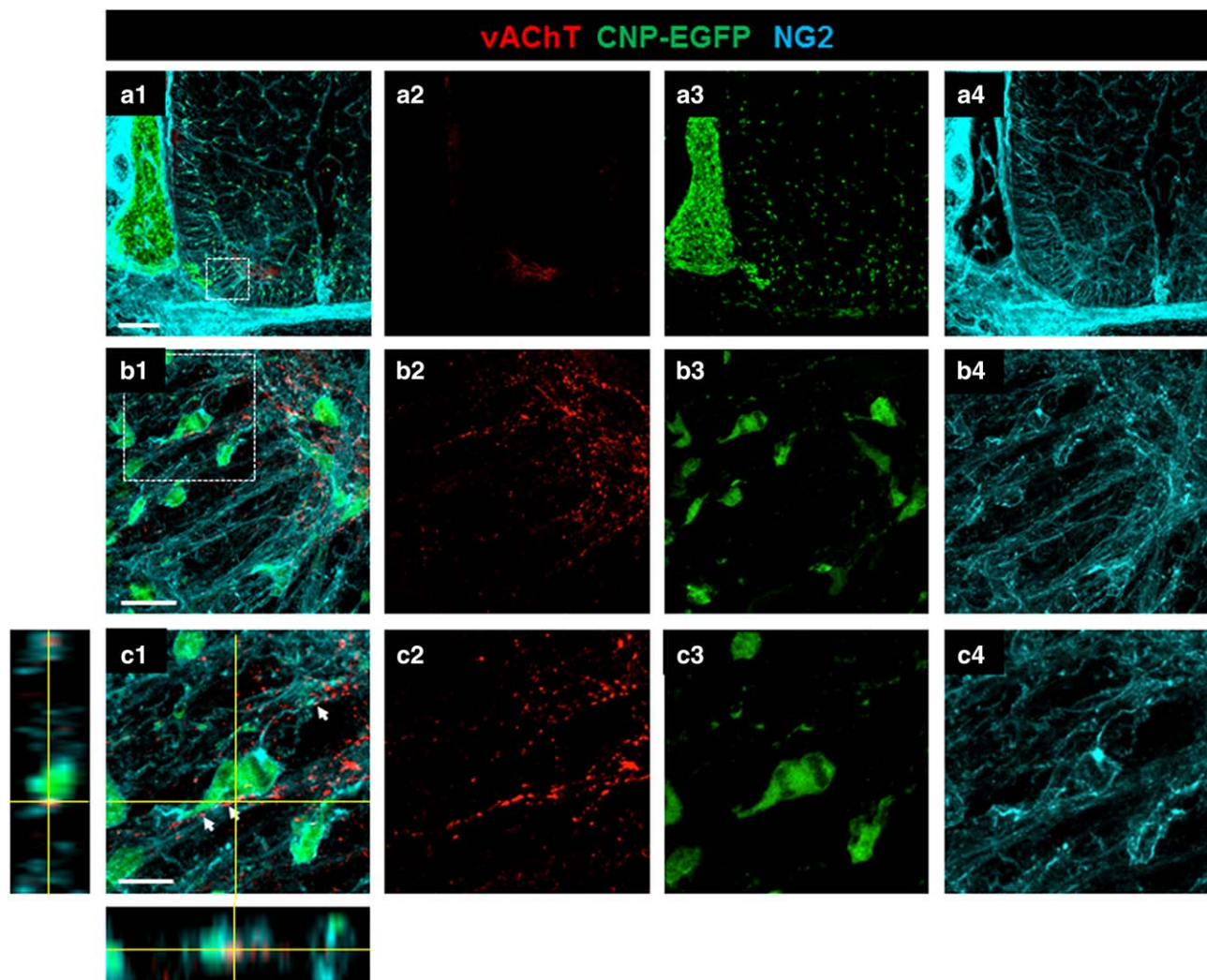
FIGURE 8 Putative acetylcholine release sites are found apposed to OPCs located in the MEP. (a1–a4) confocal images at low magnification showing the location of putative release sites for acetylcholine labelled by VAChT (in red) and pioneer OPCs labelled by CNP-EGFP (in green) and NG2 (in cyan) in a coronal section from a CNP-EGFP E14.5 mouse embryo. Note how VAChT staining is limited to the ventro-lateral parenchyma where motoneurons are located in the spinal cord. (b1–b4) confocal images of the same coronal section at a higher magnification (boxed region in a1–a4) showing the presence of VAChT$^+$ puncta (in red) in the vicinity of pioneer OPCs labelled by CNP-EGFP (in green) and NG2 (in cyan). (c1–c4) Confocal image at the highest magnification (boxed region in B1-B4) showing the presence of VAChT$^+$ puncta apposed to OPCs located at the MEP (white arrows) [Color figure can be viewed at wileyonlinelibrary.com]

endogenous cholinergic signaling regulates the activity of GABAergic axoglial synapses by acting through presynaptic nAChRs. Finally, we demonstrate that over-activation of nAChR by chronic nicotine fetal exposure leads to a significant increase in OPC density and proliferation in the ventral part of the embryonic spinal cord. Taken together, our results show that axoglial synapses are formed onto pioneer OPCs as soon as they arise from their precursor domain and that their ability to proliferate and colonize the ventral embryonic spinal cord can be altered by changes in cholinergic signaling.

4.1 | Do neuroepithelial precursors in the pMN domain directly transform into pioneer OPCs?

We show here that the first OPCs that can be identified by NG2 immunoreactivity in the pMN domain exhibit a radial morphology similar to the neuroepithelial precursors that generate them. Indeed, we show that early born NG2-positive OPCs already exhibit radial processes contacting the marginal zone and the central canal while their soma is still located in the ventricular zone. Intriguingly, we found that these NG2-positive radial processes transiently co-express the neuro-epithelial markers nestin and GLAST. We propose that either (1) neuro-epithelial precursors directly transform into OPCs or (2) neuro-epithelial precursors undergo asymmetric division to generate neuro-epithelial precursors and OPCs with similar radial morphologies that are closely associated. A number of evidence supports the former explanation. First, Fogarty et al., showed that the second wave of OPCs arising from the dbx1 domain in the dorsal spinal cord occurs by direct transformation of radial glial precursors into OPCs (Fogarty, Richardson, & Kessaris, 2005). Similar to our observation in the pMN domain, they found that OPC generation in the dbx1 domain was
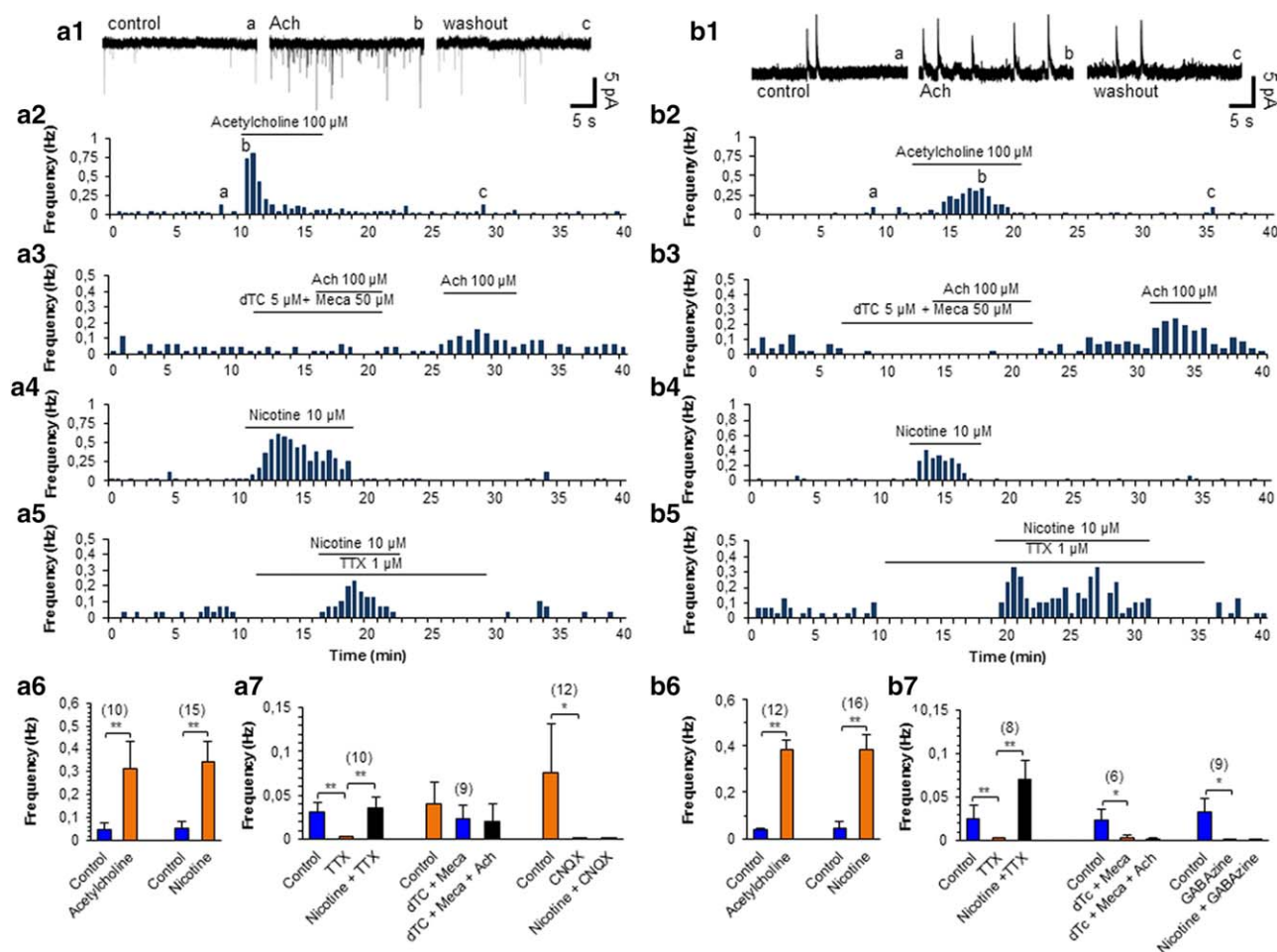
FIGURE 9 Cholinergic signaling potentiates axoglial synapses by acting onto presynaptic nicotinic acetylcholine receptors. (a1) Representative voltage-clamp recordings from a CNP-EGFP$^+$ OPC located in the MEP at E13.5. At a holding potential of -60 mV, the cell exhibited glutamatergic synaptic currents (left trace, control) that were potentiated by the application of acetylcholine (center trace, Ach 100 μM) in a reversible manner (right trace, washout). (a2–a5) Representative plots from individual cells showing the changes in instantaneous frequency of glutamatergic synaptic currents during application of acetylcholine alone (top trace, Ach 100 μM) or in presence of nAChR antagonists (second trace, Mecamylamine 50 μM + d-Tubocurarine 5 μM) as well as to nicotine alone (third trace, Nicotine 10 μM) or in presence of tetrotoxin (bottom trace, TTX 1 μM) showing that activation of presynaptic nAChR potentiates glutamate synaptic release onto pioneer OPCs. (a6 and a7) Plots summarizing the effects of these various manipulations of cholinergic signaling onto glutamatergic synaptic current frequency. (b1) Representative voltage-clamp recordings from a CNP-EGFP$^+$ OPC located in the MEP at E13.5. At a holding potential of 0 mV, the cell exhibited GABAergic synaptic currents (left trace, control) that were potentiated by the application of acetylcholine (center trace, Ach 100 μM) in a reversible manner (right trace, washout). (b2–b5) Representative plots from individual cells showing the changes in instantaneous frequency of GABAergic synaptic currents during application of acetylcholine alone (top trace, Ach 100 μM) or in presence of nAChR antagonists (second trace, Mecamylamine 50 μM + d-Tubocurarine 5 μM) as well as to nicotine alone (third trace, Nic 10 μM) or in presence of tetrotoxin (bottom trace, TTX 1 μM) showing that activation of presynaptic nAChR potentiates GABA synaptic release onto pioneer OPCs. (b6 and b7) Plots summarizing the effect of manipulating cholinergic signaling onto GABAergic synaptic currents frequency (mean, SEM). Number of independent repeats (n) for each experiment is specified in the figure. Statistical differences are as indicated (*$p < .05$, **$p < .01$) [Color figure can be viewed at wileyonlinelibrary.com]

associated with the appearance of a transient population of radial glial cells co-expressing both OPC and neuro-epithelial precursor markers. Second, we observed that the pool of olig2-expressing neuro-epithelial precursor in the pMN domain is drastically depleted at E14.5 (see Figure 1e3) right after the first wave of OPC has been generated. Taken together, these observations support the hypothesis that pMN precursors directly transform into OPCs by detaching from the ventricular zone to follow their radial process into the marginal zone. This would also explain why the soma of pioneer OPCs are preferentially found

accumulating around the MEP, where the radial processes of most of these Nestin$^+$/Olig2$^+$ precursors are initially located. Finally, we show that putative axoglial synapses can be found onto nestin-positive processes in the MZ at E12.5 while just one day later, functional axoglial synapses can be recorded in pioneer OPCs whose soma have reached the MZ. The fact that both pioneer OPCs and the neuroepithelial precursors they arise from would share such a particular feature brings further support to the hypothesis that OPCs directly transform from neuro-epithelial precursors and inherit their axoglial synapses in the
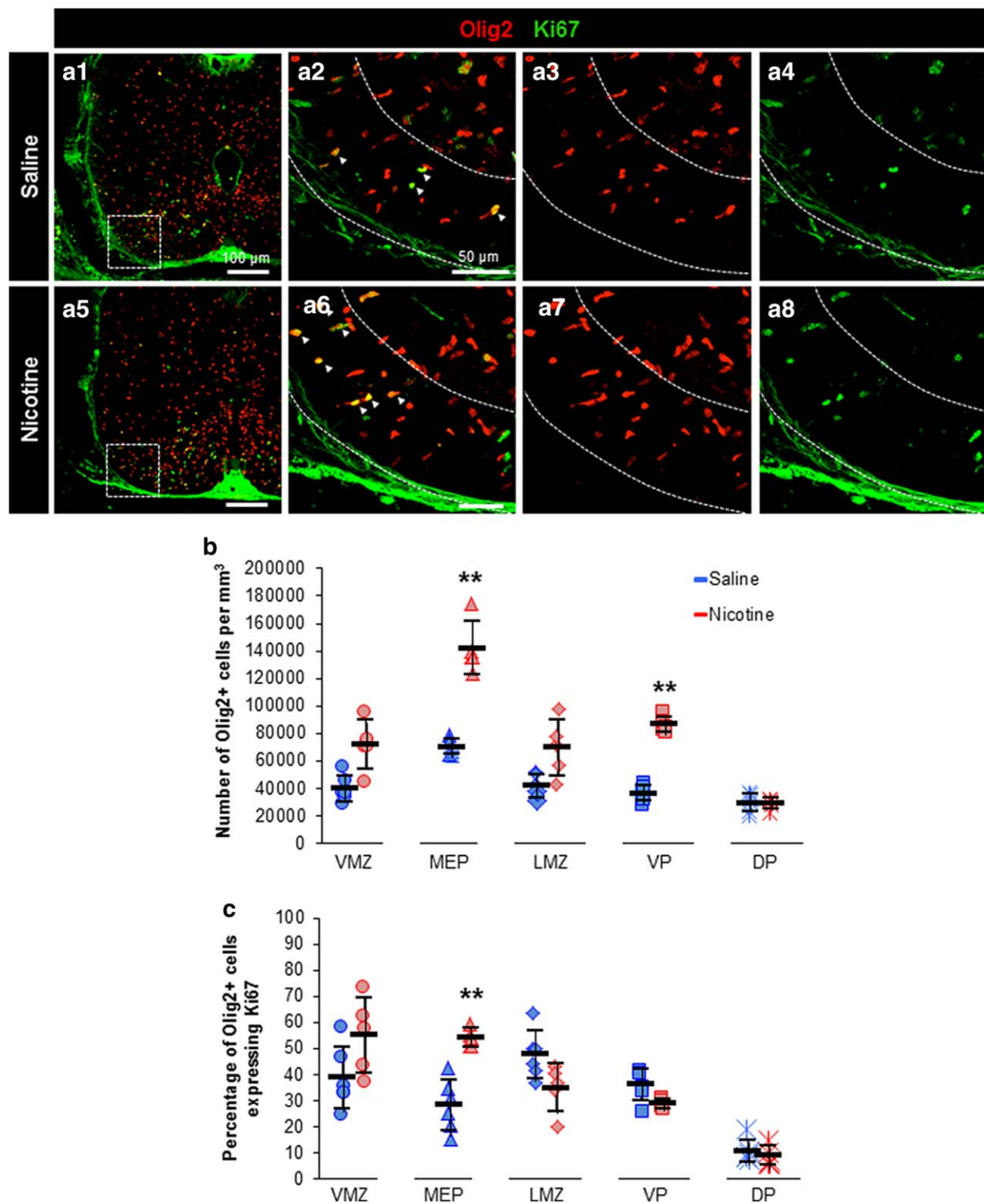
FIGURE 10 Chronic fetal nicotine exposure increases OPC density and proliferation at the motor exit point. (a) Confocal images showing immunofluorescence stainings for Olig2 (red) and Ki67 (green) in coronal sections of mouse spinal cord from E14.5 embryos. Embryos were treated from E10.5 to E14.5 stages by implanting pregnant females with osmotic pumps containing either saline (a1–a4, saline) or nicotine (a5–a8, Nicotine 10 mg/kg). Note the increased density of Olig2$^+$ cells (arrowheads) in the ventral spinal cord of nicotine-treated embryos (Scale bar = 100 μm). (b) Plots quantifying the density of Olig2$^+$ cells in different regions of the spinal cord in saline- and nicotine-treated embryos. VMZ = ventral marginal zone; MEP = motor exit point; LMZ = lateral marginal zone; VP = ventral parenchyma; DP = dorsal parenchyma (For the exact location of each area quantified, see drawing in Figure 1c1). The density of Olig2$^+$ cells was significantly increased in the MEP and the VP of nicotine-treated embryos. (c) Plots quantifying the ratio of Ki67$^+$/Olig2$^+$ cells in different regions of the spinal cord in saline- and nicotine-treated embryos. The proliferation rate of Olig2$^+$ cells was significantly increased in the MEP of nicotine-treated embryos. Statistical differences (ns, not significant, *$p < .05$, **$p < .01$) are shown [Color figure can be viewed at wileyonlinelibrary.com]

process. In contrast, some evidence also support the second hypothesis —that is that the nestin-positive and NG2-positive radial processes found in the MZ belong to distinct but closely associated cell populations. This hypothesis is favored by Diers-Fenger and colleagues who showed in E15 mouse spinal cord that processes stained with AN2/NG2 antibodies were closely associated to radial glial processes stained with Nestin (Diers-Fenger, Kirchhoff, Kettenmann, Levine, & Trotter, 2001).

4.2 | Could the onset of synaptogenesis trigger OPC specification?

Our present work suggests that axoglial synapses are a universal and defining property of OPCs, regardless of their location (brain vs. spinal cord) or developmental stages (embryonic vs. postnatal). Indeed, axoglial synapses are known to disappear as soon as OPCs differentiate into oligodendrocytes (De Biase et al., 2010; Etxeberria et al., 2010; Kukley et al., 2010) and we now show that they are also formed as soon as OPCs are generated during embryonic development. More importantly, our work suggests that axoglial synapses may even participate to trigger, or at least regulate, OPC genesis from neuroepithelial precursors. Indeed, electron microscopy show that the emergence of OPCs from neuro-epithelial precursors is concomitant with the formation of synaptic-like axoglial contacts onto neuro-epithelial precursors glial processes located in the marginal zone (see Figure 7; Henrikson & Vaughn, 1974). Moreover, our results suggest that the potentiation of glutamatergic and/or GABAergic axoglial transmission by nicotine could not only favor the secondary proliferation of pioneer OPCs in the marginal zone surrounding the MEP, but also facilitate the recruitment of neuro-epithelial precursors into OPC. Indeed, we observed that fetal nicotine exposure could increase OPC density in the ventral parenchyma without any increase in their local proliferation rate (see Figure 10). Therefore, these supernumerary parenchymal OPCs must have been generated elsewhere. Because they are located along the path likely to be taken by most pioneer OPCs right after they leave the pMN domain, their most likely origin would therefore be the pMN domain itself. Indeed, they are located along the path traced by NG2/nestin radial glial endfeets at E12.5 (see Figures 1a and 2) and we showed that pioneer OPCs transiently accumulate in the ventral parenchyma at E13.5 before colonizing the marginal zone at E14.5 (see Figure 1e2).

We hypothesize that the formation of axoglial synapses allow glial precursors to insure that the neuronal components of the ventral spinal motor network have been properly connected and are functional before initiating gliogenesis. Indeed, it has long been known that ventral spinal motor networks start exhibiting bursts of spontaneous neuronal activity (SNA) around E12.5 in mouse embryos (Hanson, Milner, & Landmesser, 2008) when the first OPC are specified. We previously showed that SNA triggers the release of acetylcholine from MNs and the release of GABA and glutamate from spinal interneurons (Czarnecki et al., 2014). We show here that pioneer OPCs could directly detect GABA and glutamate released during SNA through their axoglial synapses and indirectly detect acetylcholine by its action onto the presynaptic nAChRs. Therefore, SNA and axoglial synapses could act as a

feedback mechanism linking the onset of gliogenesis to the functional maturity of the developing spinal cord neuronal network.

To further investigate whether axoglial synapses are indeed systematically formed at the onset of gliogenesis, it would be of great interest to explore the other areas of the central nervous system known to generate OPCs during embryonic development (Richardson, Kessaris, & Pringle, 2006). For example, the second wave of OPCs generated by radial glia in the dorsal spinal cord (Bilican, Fiore-Heriche, Compston, Allen, & Chandran, 2008; Fogarty et al., 2005; Vallstedt, Klos, & Ericson, 2005) is correlated with the onset of synaptogenesis in the dorsal marginal zone when peripheral sensory inputs enter the dorsal spinal cord (Marmigère & Ernfors, 2007).

In conclusion, we demonstrated for the first time that OPCs are contacted by functional synapses as soon as they emerge from their precursor domain and that embryonic spinal cord invasion by OPCs can be regulated by cholinergic signaling acting onto these axoglial synapses, revealing new functional developmental mechanisms during the formation of the spinal cord network.

AUTHOR CONTRIBUTIONS

G. Osterstock designed, performed and analyzed all electrophysiogical, fetal nicotine treatment and most immunohistochemistry experiments. B. Lebras designed, performed and analyzed electron microscopy experiments. K. Arulkandarajah performed additional immunohistochemistry experiments. H. Le Corronc and A. Czarnecki participated to the design and analysis of electrophysiological experiments. C. Mouffle and E. Bullier managed the animal colony, performed animal genotyping and contributed to immuno-histochemistry experiments. J-M Mangin participated to the design and analysis of the experiments, supervised the whole project with P. Legendre and wrote the manuscript with G. Osterstock and P. Legendre.

ORCID

Pascal Legendre http://orcid.org/0000-0002-5086-4515
Jean-Marie Mangin http://orcid.org/0000-0002-7804-0251

REFERENCES

Arias, H. R., Rosenberg, A., Targowska-Duda, K. M., Feuerbach, D., Jozwiak, K., Moaddel, R., & Wainer, I. W. (2010). Tricyclic antidepressants and mecamylamine bind to different sites in the human $\alpha4\beta2$ nicotinic receptor ion channel. *The International Journal of Biochemistry & Cell Biology, 42* (6), 1007–1018. http://doi.org/10.1016/j.biocel.2010.03.002

Barry, D. S., Pakan, J. M. P., O'Keeffe, G. W., & McDermott, K. W. (2013). The spatial and temporal arrangement of the radial glial scaffold suggests a role in axon tract formation in the developing spinal cord. *Journal of Anatomy*, *222*(2), 203–213. http://doi.org/10.1111/joa.12006

Bergles, D. E., & Richardson, W. D. (2016). Oligodendrocyte Development and Plasticity. *Cold Spring Harbor Perspectives in Biology*, *8*(2), a020453. http://doi.org/10.1101/cshperspect.a020453

Bergles, D. E., Roberts, J. D., Somogyi, P., & Jahr, C. E. (2000). Glutamatergic synapses on oligodendrocyte precursor cells in the hippocampus. *Nature*, *405*(6783), 187–191. http://doi.org/10.1038/35012083

Bernard, V., Levey, A. I., & Bloch, B. (1999). Regulation of the subcellular distribution of m4 muscarinic acetylcholine receptors in striatal neurons in vivo by the cholinergic environment: Evidence for regulation of cell surface receptors by endogenous and exogenous stimulation. *The Journal of Neuroscience : The Official Journal of the Society for Neuroscience*, *19*(23), 10237–10249. Retrieved from http://www.ncbi.nlm.nih.gov/pubmed/10575021

Bilican, B., Fiore-Heriche, C., Compston, A., Allen, N. D., & Chandran, S. (2008). Induction of Olig2 precursors by FGF involves BMP signalling blockade at the Smad level. *PloS One*, *3*(8), e2863. http://doi.org/10.1371/journal.pone.0002863

Czarnecki, A., Le Corronc, H., Rigato, C., Le Bras, B., Couraud, F., Scain, A.-L., . . . Legendre, P. (2014). Acetylcholine controls GABA-, glutamate-, and glycine- dependent giant depolarizing potentials that govern spontaneous motoneuron activity at the onset of synaptogenesis in the mouse embryonic spinal cord. *Journal of Neuroscience*, *34*(18), 6389. http://doi.org/10.1523/JNEUROSCI.2664-13.2014

De Biase, L. M., Nishiyama, A., & Bergles, D. E. (2010). Excitability and synaptic communication within the oligodendrocyte lineage. *Journal of Neuroscience*, *30*(10), 3600–3611. http://doi.org/10.1523/JNEUROSCI.6000-09.2010

Diers-Fenger, M., Kirchhoff, F., Kettenmann, H., Levine, J. M., & Trotter, J. (2001). AN2/NG2 protein-expressing glial progenitor cells in the murine CNS: Isolation, differentiation, and association with radial glia. *Glia*, *34*(3), 213–228. Retrieved from http://www.ncbi.nlm.nih.gov/pubmed/11329183

Dumoulin, A., Rostaing, P., Bedet, C., Lévi, S., Isambert, M. F., Henry, J. P., . . . Gasnier, B. (1999). Presence of the vesicular inhibitory amino acid transporter in GABAergic and glycinergic synaptic terminal boutons. *Journal of Cell Science*, 811–823. Retrieved from http://www.ncbi.nlm.nih.gov/pubmed/10036231

Etxeberria, A., Mangin, J.-M., Aguirre, A., & Gallo, V. (2010). Adult-born SVZ progenitors receive transient synapses during remyelination in corpus callosum. *Nature Neuroscience*, *13*(3), 287. http://doi.org/10.1038/nn.2500

Fogarty, M., Richardson, W. D., & Kessaris, N. (2005). A subset of oligodendrocytes generated from radial glia in the dorsal spinal cord. *Development (Cambridge, England)*, *132*(8), 1951–1959. http://doi.org/10.1242/dev.01777

Gallo, V., Mangin, J.-M., Kukley, M., & Dietrich, D. (2008). Synapses on NG2-expressing progenitors in the brain: Multiple functions? *The Journal of Physiology*, *586*(16), 3767. http://doi.org/10.1113/jphysiol.2008.158436

Hanson, M. G., & Landmesser, L. T. (2003). Characterization of the circuits that generate spontaneous episodes of activity in the early embryonic mouse spinal cord. *The Journal of Neuroscience : The Official Journal of the Society for Neuroscience*, *23*(2), 587–600. Retrieved from http://www.ncbi.nlm.nih.gov/pubmed/12533619

Hanson, M. G., Milner, L. D., & Landmesser, L. T. (2008). Spontaneous rhythmic activity in early chick spinal cord influences distinct motor axon pathfinding decisions. *Brain Research Reviews*, *57*(1), 77–85. http://doi.org/10.1016/j.brainresrev.2007.06.021

Henrikson, C. K., & Vaughn, J. E. (1974). Fine structural relationships between neurites and radial glial processes in developing mouse spinal cord. *Journal of Neurocytology*, *3*(6), 659–675. Retrieved from http://www.ncbi.nlm.nih.gov/pubmed/4461770

Herzog, E., Bellenchi, G. C., Gras, C., Bernard, V., Ravassard, P., Bedet, C., . . . El Mestikawy, S. (2001). The existence of a second vesicular glutamate transporter specifies subpopulations of glutamatergic neurons. *The Journal of Neuroscience : The Official Journal of the Society for Neuroscience*, *21*(22), RC181. Retrieved from http://www.ncbi.nlm.nih.gov/pubmed/11698619

Hill, R. A., & Nishiyama, A. (2014). NG2 cells (polydendrocytes): Listeners to the neural network with diverse properties. *Glia*, *62*(8), 1195–1210. http://doi.org/10.1002/glia.22664

Jefferys, J. G. (1995). Nonsynaptic modulation of neuronal activity in the brain: Electric currents and extracellular ions. *Physiological Reviews*, *75*(4), 689–723. http://doi.org/10.1152/physrev.1995.75.4.689

Jonsson, M., Gurley, D., Dabrowski, M., Larsson, O., Johnson, E. C., & Eriksson, L. I. (2006). Distinct pharmacologic properties of neuromuscular blocking agents on human neuronal nicotinic acetylcholine receptors: A possible explanation for the train-of-four fade. *Anesthesiology*, *105*(3), 521–533. Retrieved from http://www.ncbi.nlm.nih.gov/pubmed/16931985

Kukley, M., Capetillo-Zarate, E., & Dietrich, D. (2007). Vesicular glutamate release from axons in white matter. *Nature Neuroscience*, *10*(3), 311–320. http://doi.org/10.1038/nn1850

Kukley, M., Nishiyama, A., & Dietrich, D. (2010). The fate of synaptic input to NG2 glial cells: Neurons specifically downregulate transmitter release onto differentiating oligodendroglial cells. *The Journal of Neuroscience : The Official Journal of the Society for Neuroscience*, *30*(24), 8320–8331. http://doi.org/10.1523/JNEUROSCI.0854-10.2010

Lin, S.-C., & Bergles, D. E. (2004). Synaptic signaling between neurons and glia. *Glia*, *47*(3), 290–298. http://doi.org/10.1002/glia.20060

Lin, S., & Bergles, D. E. (2004). Synaptic signaling between GABAergic interneurons and oligodendrocyte precursor cells in the hippocampus. *Nature Neuroscience*, *7*(1), 24–32. http://doi.org/10.1038/nn1162

Mangin, J.-M., Kunze, A., Chittajallu, R., & Gallo, V. (2008). Satellite NG2 progenitor cells share common glutamatergic inputs with associated interneurons in the mouse dentate gyrus. *The Journal of Neuroscience : The Official Journal of the Society for Neuroscience*, *28*(30), 7610–7623. http://doi.org/10.1523/JNEUROSCI.1355-08.2008

Marmigère, F., & Ernfors, P. (2007). Specification and connectivity of neuronal subtypes in the sensory lineage. *Nature Reviews. Neuroscience*, *8*(2), 114–127. http://doi.org/10.1038/nrn2057

Matta, S. G., Balfour, D. J., Benowitz, N. L., Boyd, R. T., Buccafusco, J. J., Caggiula, A. R., . . . Zirger, J. M. (2007). Guidelines on nicotine dose selection for in vivo research. *Psychopharmacology*, *190*(3), 269–319. http://doi.org/10.1007/s00213-006-0441-0

Nishiyama, A., Lin, X. H., Giese, N., Heldin, C. H., & Stallcup, W. B. (1996). Co-localization of NG2 proteoglycan and PDGF alpha-receptor on O2A progenitor cells in the developing rat brain. *Journal of Neuroscience Research*, *43*(3), 299–314. http://doi.org/10.1002/(SICI)1097–4547(19960201)43:3<299::AID-JNR5>3.0.CO;2-E

Paukert, M., & Bergles, D. E. (2006). Synaptic communication between neurons and NG2+ cells. *Current Opinion in Neurobiology*, *16*(5), 515–521. http://doi.org/10.1016/j.conb.2006.08.009

Pringle, N. P., & Richardson, W. D. (1993). A singularity of PDGF alpha-receptor expression in the dorsoventral axis of the neural tube may define the origin of the oligodendrocyte lineage. *Development (Cambridge, England)*, *117*(2), 525–533. Retrieved from http://www.ncbi.nlm.nih.gov/pubmed/8330523

Richardson, W. D., Kessaris, N., & Pringle, N. (2006). Oligodendrocyte wars. *Nature Reviews. Neuroscience*, *7*(1), 11–18. http://doi.org/10.1038/nrn1826

Ross, E. J., Graham, D. L., Money, K. M., & Stanwood, G. D. (2015). Developmental consequences of fetal exposure to drugs: What we know and what we still must learn. *Neuropsychopharmacology*, *40*(1), 61–87. http://doi.org/10.1038/npp.2014.147

Rowitch, D. H. (2004). Glial specification in the vertebrate neural tube. *Nature Reviews. Neuroscience*, *5*(5), 409–419. http://doi.org/10.1038/nrn1389

Sahel, A., Ortiz, F. C., Kerninon, C., Maldonado, P. P., Angulo, M. C., & Nait-Oumesmar, B. (2015). Alteration of synaptic connectivity of oligodendrocyte precursor cells following demyelination. *Frontiers in Cellular Neuroscience*, *9*, 77. http://doi.org/10.3389/fncel.2015.00077

Scain, A.-L., Le Corronc, H., Allain, A.-E., Muller, E., Rigo, J.-M., Meyrand, P., . . . Legendre, P. (2010). Glycine release from radial cells modulates the spontaneous activity and its propagation during early spinal cord development. *The Journal of Neuroscience : The Official Journal of the Society for Neuroscience*, *30*(1), 390–403. http://doi.org/10.1523/JNEUROSCI.2115-09.2010

Shibata, T., Yamada, K., Watanabe, M., Ikenaka, K., Wada, K., Tanaka, K., & Inoue, Y. (1997). Glutamate transporter GLAST is expressed in the radial glia-astrocyte lineage of developing mouse spinal cord. *The Journal of Neuroscience : The Official Journal of the Society for Neuroscience*, *17*(23), 9212–9219. Retrieved from http://www.ncbi.nlm.nih.gov/pubmed/9364068

Vallstedt, A., Klos, J. M., & Ericson, J. (2005). Multiple dorsoventral origins of oligodendrocyte generation in the spinal cord and hindbrain. *Neuron*, *45*(1), 55–67. http://doi.org/10.1016/j.neuron.2004.12.026

Vaughn, J. E., Henrikson, C. K., & Grieshaber, J. A. (1974). A quantitative study of synapses on motor neuron dendritic growth cones in developing mouse spinal cord. *The Journal of Cell Biology*, *60*(3), 664–672. Retrieved from http://www.ncbi.nlm.nih.gov/pubmed/4824291

Yuan, X., Chittajallu, R., Belachew, S., Anderson, S., McBain, C. J., & Gallo, V. (2002). Expression of the green fluorescent protein in the oligodendrocyte lineage: A transgenic mouse for developmental and physiological studies. *Journal of Neuroscience Research*, *70*(4), 529–545. http://doi.org/10.1002/jnr.10368

Ziskin, J. L., Nishiyama, A., Rubio, M., Fukaya, M., & Bergles, D. E. (2007). Vesicular release of glutamate from unmyelinated axons in white matter. *Nature Neuroscience*, *10*(3), 321–330. http://doi.org/10.1038/nn1854